Computers and Electrical Engineering 74 (2019) 35–46

Contents lists available at ScienceDirect

Computers and Electrical Engineering

journal homepage: www.elsevier.com/locate/compeleceng

Cloud enhancement of NOAA multispectral images by using independent component analysis and principal component analysis for sustainable systems☆

T. Venkatakrishnamoorthy*, G. Umamaheswara Reddy

Department of Electronics and Communication Engineering, Sri Venkateswara University College of Engineering, SV University, Tirupati 517501, Andhra Pradesh, India

ARTICLE INFO

Article history:
Received 10 September 2018
Revised 14 December 2018
Accepted 15 January 2019
Available online 18 January 2019

Keywords:
Multispectral image
Independent component analysis
Skew and Kurtosis
principal component analysis
Non-Gaussian
Spatial and spectral information

ABSTRACT

Multispectral (MS) images, which display spectral and spatial information, play a vital role in remote sensing applications for analysing objects. This paper focuses on the spatial and spectral enhancement of cloud objects through the fusion technique. The complete information is represented in limited bands through independent component analysis and principal component analysis. The objects of MS images do not have the same quality in all individual bands. Instead of a selection of individual bands, the complete information about input image obtained by limited bands with skew- and kurtosis-based ICA transforms, it is suitable for non-Gaussian application in the satellite image. In preprocessing, the spatial and spectral information is lost due to the low resolution of individual bands. The information is recovered from the high-resolution first principal component of the MS image. The classification was performed using k-means clustering, and accurate values were obtained with the proposed method. This method gives a good tradeoff between the spectral and spatial information and superior accuracy results compared with other enhancement and fusion methods.

1. Introduction to remote sensing and its applications

Remote sensing is the process of analysing, recording, and measuring information regarding a phenomenon from a distance without any physical human interaction. Active and passive sensors are used for acquiring information regarding objects on the earth or in the atmosphere. In the active sensing, a signal is emitted by the satellite and reflected by the object, whereas in passive sensing, sunlight is detected by the sensor. Thus, passive sensors depend on an external source. The Capturing information depends on the number of bands or channels used in image processing, such as panchromatic, multispectral (MS), and hyper spectral. In 1970, infrared (IR) sensors were added to satellites for image acquisition during both night and day. Many applications can be performed through remote sensing, [29] including image classification, spectral analysis, and orthorectification with specialized file formats such as Geo-tiff, JPEG2000, NITF, and Net CDF [1].

Satellite MS images cover a wide range of the electromagnetic spectrum and include visible, IR, reflected, and Thermal channels. There exists accurate discrimination between similar bands. Using the MS image directly in image processing ap-

☆ This paper is for CAEE special section SI-scss. Reviews processed and recommended for publication to the Editor-in-Chief by Guest Editor Dr. A.P. Pandian.

* Corresponding author.
E-mail address: krishna454@gmail.com (T. Venkatakrishnamoorthy).

https://doi.org/10.1016/j.compeleceng.2019.01.005
0045-7906/

plications is a computationally expensive process. Moreover, the small ratio between the availability of training samples and the spectral dimensions results in a decrease in the overall accuracy of classification. NOAA-AVHRR bands contain considerable repeated information in their bands. Therefore, all the bands are not required for a certain applications. Reduction of information and size is important because redundancy increases the storage space required by and computational burden of applications. NOAA prefers optical remote sensing for capturing land objects and clouds. Images are formed by visible, IR, and near-IR sensors through the solar radiation reflected from objects on the earth's surface or in the atmosphere. Clouds are playing a vital role in the earth's hydrologic cycle. Clouds are assumed to be homogeneous, flat, and infinite slabs. The Clouds are very sensitive to global changes in the surface temperature. The visible, IR, and thermal channels are helpful for analysing the cloud information in MS NOAA-19 satellite images. NOAA images are useful for finding climate, weather changes, disaster warnings and improve weather forecasting.

Image processing techniques are mostly used for feature extraction of color images, Texture based segmentation is a difficult problem, it depends on pixel resolution and knowledge of which type of texture is available at that position, the same object pixel also visible as different resolution in different channels, same redundancy appearing in MS images [15,16]. Color normal techniques, false color composite models Red, Green and Blue channels are used in transforming method, due to selection of bands in MS image this technique doesn't give sophisticated results [13]. In Spatial domain fusion techniques are simple for enhanced the spatial information, so in this pixel due to lack of contrast information the image appears as blur, Transform domain fusion methods are very complex, loss the trade off between spatial and spectral components [19]. Histogram Equalization technique the total image intensities are distributed equally, if the problem will occur with external disturbance like atmospheric conditions and sensor poor capturing, we will get another information instead of original information. [9,25]

Unsupervised/classification can be done for satellite images, the satellite images contain low resolution and multiple bands, the classification for each band is very difficult and not getting ideal bands from sensors, so these bands reduced redundancy multiple bands into useful information bands using dimensional reduction with dimensional reduction techniques. PCA is one of the best technique, it is based on 2D matrices, using covariance matrix is constructed directly using the original image matrices instead if using 1D matrix need not transformed before prior to extracting data [21,24].

ICA is a linear transformation technique for non-Gaussian applications. ICA involves higher-order statistical (skew and kurtosis) features extraction, where the asymmetry in and flatness of the histogram is measured. ICA is the one of the statistical technique for better decomposing a complex dataset (more band set image) into independent subparts. It develops from blind source separation and attempts to transform an observed multidimensional vector into components that are statistically independent from each other as much as possible.

In this paper, Section 2 presents the dimensionality reduction process using ICA and PCA techniques for image enhancement. In Section 3, focuses on the proposed method and supervised/unsupervised classifications. Results are discussed and compared with different pan sharpening methods and cloud separation methods using clustering based supervised/unsupervised techniques are dealt Section 4. Finally, Section 5 deals with a conclusion and future scope.

2. Dimensional reduction (DR) using ICA and PCA

MS NOAA images typically contain spatial and statistical information in all bands, more repeated data available in all bands. There exist a high number of correlation coefficients between bands, Enhanced satellite image scenes can be decomposed into various features by using digital image processing [32,31], without the loss of spectral characteristics in remote sensing applications, such as vegetation, temperature, cloud types, and urban materials. These retrieves features with a good accuracy level, which are useful for improving the performance of remote sensing applications. Dimensionality reduction is one approach for the PCA of MS images [2,10]. In PCA, the precedence order is followed for the components. Maximum data variance is available in the first component; the variance of second-highest data is available in the second component, and so on. However, ICA does not imply any order. Moreover, the components (axis) are not restricted to the orthogonal, and the transformed data are independent. The component values do not contain any similar information. Thus, the components are mutually independent (orthogonal) to each other. The main disadvantage of PCA is that the abatement of the discrimination information present in the original feature space is not always guaranteed and not provides better discrimination than the original feature subset. With regard to the minimum noise fraction, PCA provides satisfactory results for Gaussian distribution only. However, most remote sensing images do not follow Gaussian operations. Fast ICA is a statistical method for DR. In fast ICA [12], data are linearly transformed from a large to a low-dimensional space. Features are extracted and redundant information is discarded to improve the efficiency of the classification stage. This paper provides practical information regarding the use of MS images in higher-order statistics ICA, DR, blind source separation, and decomposing a multivariate signal into an independent non-Gaussian IC components.

ICA transformation bands are independent, and each IC component contains a specific feature of the MS image scene. The ordering option of ICA for MS image can be followed with HOS as skew and kurtosis [26]. This operation can be performed using eigenvectors. By using the covariance or correlation matrix, the redundant data are identified, and eigenvectors for the independent components of the input satellite image are used to reconstruct the large fraction of variance of the MS image. First, three eigenvectors from Fig. 1 (IC1, IC2, and IC3) are interpreted as the reduction between the different band images of the original space. A maximum of 96.6% information is covered in first few IC components. The main advantage

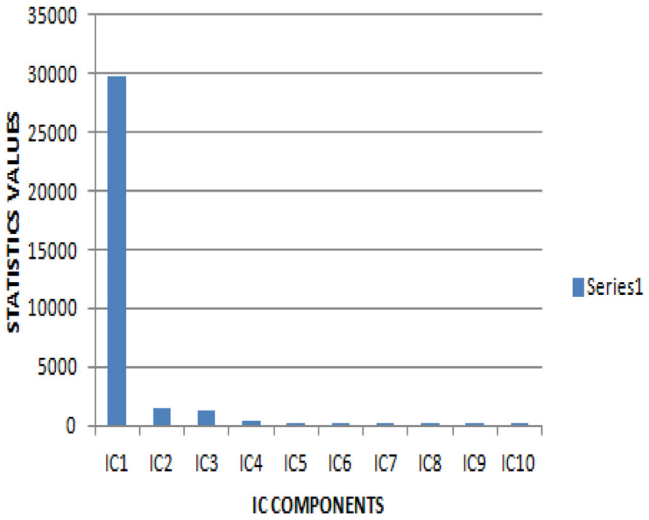

Fig. 1. DR variance plot with ICA.

Table 1a
Statistical components (IC components) of MS-images.

29721.71	IC1
1373.239	IC2
1221.743	IC3
308.1352	IC4
213.3819	IC5
111.4751	IC6
8.280245	IC7
6.505585	IC8
6.340994	IC9
Eigen vectors	IC components

of performing ICA for MS images is that the high-directional and preserved edges of an object prefer natural scenes. Edges are fundamentally built into natural scenes. The natural information is minimized, or the non-gaussianity is maximized.

3. Methodology

ICA transforms were used to extract the spatial and spectral features of satellite cloud data in the IC1, IC2, and IC3 channels. The clouds could be classified as high, low, and medium-level clouds, which were formed by water or ice particles [3].

Considerable research has been conducted on cloud classification based on spectral, spatial, and textural features. In classification based on spatial and spectral features [20], object information is extracted according to the spectral band radiance, threshold scheme, histogram, and the MS approach [22]. With spectral features such as albedo (reflectance) and surface temperature, the problem of snow, ice, and water-level clouds are encountered [8]. By using textural features, different types of clouds can be distinguished according to the spatial distribution characteristics of the gray levels corresponding to a region in one specific channel. Numerous methods have been used in texture-based cloud classification, such as the gray-level co-occurrence matrix, gray-level difference vector, gray-level difference matrix, and the sum and difference histogram methods and fuzzy and neural networks. NOAA-AVHRR MS imaging sensors provide a large number of spectral bands [17,30].. This vector space dimension is represented by the number of spectral bands. Large dimensional data have a poor capability and response for supervised and unsupervised classification due to the selection of a large number of training samples.

Fig. 1 and Table 1a show the first IC statistical component values are more than 95% values compare with total image. The joint probability density and entropy can be expressed as follows:

$$X = AS \tag{1}$$

$$\mathrm{W} = \mathrm{A}^{-1} \tag{2}$$

$$\mathrm{S}_{\mathrm{est}} = \mathrm{W}_{\mathrm{x}} \tag{3}$$

The matrix (W) and sources (S_{est}) can be estimated from the observed vector signals.
X: observed vector signals
A: scalar matrix coefficients
S: source vector signals

The components of the vector signals (s_i) have a statistically independent and non-Gaussian distribution. The original multiple bands are decreased using the eigenvalues of the covariance matrix, which are related to the independence and non-gaussianity due to the central limit theorem. The eigenvalues indicate the sum of the independent random variables and change the Gaussian distribution of those variables. The estimation of ICA depends on the weights of the matrix W. Therefore, Eq. (3) Compresses the minimum number of Gaussian components. Non-gaussianity requires an optimization algorithm, and it can be measured from the kurtosis of the fourth order moment.

The entropy of a random vector is obtained as follows:

$$P(s_1, s_{2,} \ldots s_i) = \pi \ \mathrm{psi}(u_i) \tag{4}$$

$$H(px) = -\int p_x(u) \log p_x(u) du \tag{5}$$

The negentropy is measured for the entropy deficit observed for the random variable and Gaussian random vector.

$$J(x) = H(px_g) - H(px) \tag{6}$$

The negentropy is estimated as follows:

$$J(x) = \{E[G(x)] - E[G(x_g)]\} \tag{7}$$

For obtaining matrix W, the following optimization algorithm is used:

$$w+ = E\left\{xg\left(w^T x\right)\right\} - E\left\{g'\left(w^T x\right)\right\} w \tag{8}$$

w: initial weight vector
$g(u) = \tanh(u)$

$$w = w^+ / ||w + || \tag{9}$$

After every iteration, S_{est} is decorrelated using the matrix W.

$$W = \left(WW^T\right)^{-1/2} W \tag{10}$$

Here, the vector matrix $(W) = (w_1, w_2, w_3 \ldots . w_n)^T$, and
The Eigen decomposition of W is given as $= (WW^T)^{-1/2}$

3.1. Steps of the proposed algorithm

1. Collect the NOAA-AVHRR data from the L-band receiver station.
2. Select the area of interest and perform the geometric and radiometric errors.
3. Apply ICA and PCA for the MS images,
4. Perform histogram equalization for the PC1 and IC1 components to enhance the low- and high-feature components.
5. Apply inverse transform for reconstructing the image.
6. Compare the spatial and spectral qualities of different enhancement technique with suitable parameters.

3.2. Supervised and unsupervised classification

Two major types of quantitative classifications are used in remote sensing, namely supervised and unsupervised classification. Both classifications require a spectral signature for each class. The spectral signature can be obtained by selecting a sample sits for training. The selection of samples for training sites is based on software analysis in unsupervised classification. The computer can classify some classes by using the clustering algorithm [18]. Pixels are not required to be identified by the user. The identification is performed using, homogeneity criteria. Uniform pixels can be categorized as a one object.

In supervised classification, users select samples according to their knowledge to obtain the training area. After obtaining the training set, the classification is performed using the clustering principle. The user sets the spectral characteristics bounds, which determine the similarity required by two pixels to be grouped together and the number of classes. Sometimes, both supervised and unsupervised classifications are performed for classifying each and every object to improve the accuracy results. In these two classification algorithms, the computer assigns pixels to the nearest class based on the training data.

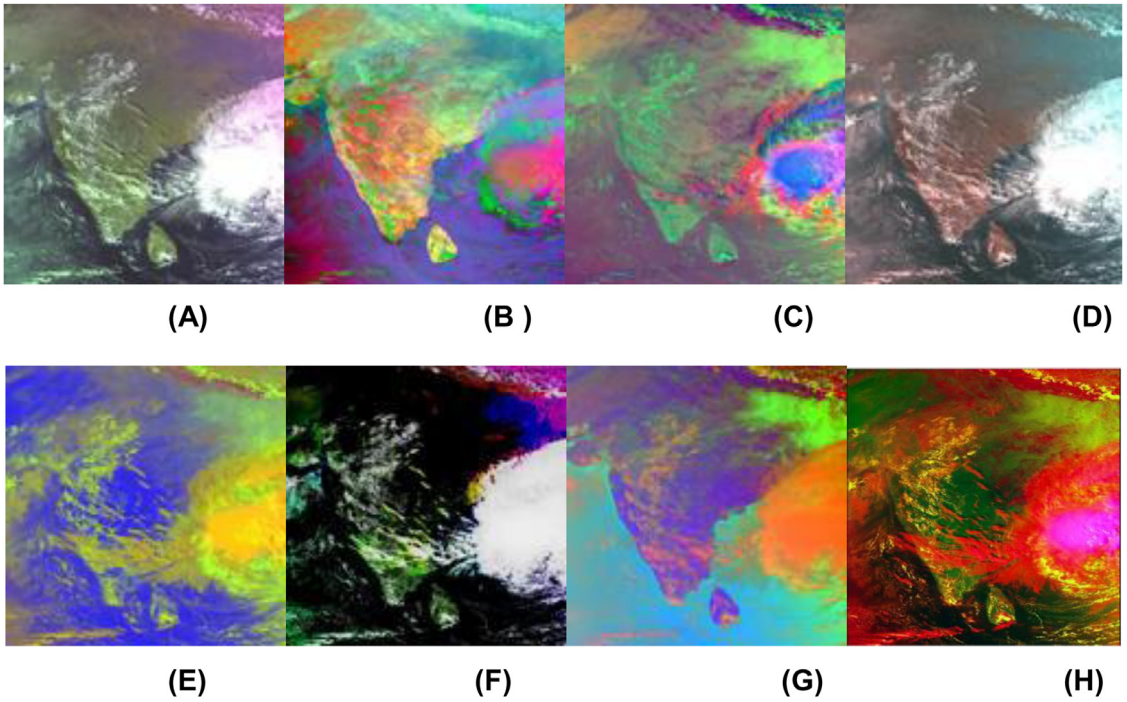

Fig. 2. (A) Input image, (B) PCA image, (C) ICA image, (D) false colour composite, (E) resolution merges, (F) Brovey transform, (G) IHS transform, and (H) proposed method.

3.3. Steps in supervised classification

1. Select the area of interest of the proposed enhanced image.
2. Select the training sets.
3. Specify the training sets to be used for the classification.
4. Apply the supervised and unsupervised classification algorithm.
5. Assess the accuracy by using the random sample point test for the classified image.

In this study, classification was performed using the k-means algorithm for unsupervised/supervised clustering of a heterogeneous population into homogeneous (similarity) groups of objects.

4. Results and discussions

There exist many methods for the spatial and spectral enhancement of the MS images. Fig. 1B illustrates the output of PCA. However, due to limited directionality, the figure lacks some information. PCA can be applied to compress and fusion operations for MS images [11]. Fig. 1D displays the false color composite, which depends on the selection of R ,G, and B channels. The Brovey transform (Fig. 1F) has limited strictly three channels. In the resolution merges (Fig. 1E), the selection of high-resolution images is difficult over all the bands. Fig. 1G depicts the HIS transform, which has more control over the color enhancement than the ICA and proposed methods. However, the ICA and proposed methods provide a higher spatial and spectral resolution than the HIS transform.

Fig. 2 illustrates the output techniques of the enhanced images. The corresponding spatial and spectral parameter values are provided in Table 1b. The proposed method provides superior parameter values compared with traditional pan-sharpening methods, such as resolution merge, PCA, and HIS. ICA provides good results. However, due to the limitations of ICA, ICA is not directly applied for DR. The limitations of ICA are overcome using PCA and histogram matching. For convincing image spatial and spectral quality with the bias, ERGS, RASE, and RMSE indices [27]. These values must be very low; however, the Q-factor and the CC values must be high. The entropy values with the proposed method are approximately equal to the input entropy value. A high correlation coefficient between the original image and processed image indicates low color distortion in the processed image.

Table 1b
Spatial and spectral parameters with the different pan-sharpening techniques.

	Resolution merge	PCA	IHST	Brovey-ICA	DWT-ICA	ICA-enhanced	ICA-IHS	ICA	Proposed
Bias	−0.0082	−0.0323	−0.0208	0.6123	0.0112	0.0029	0.0048	0.0111	0.001191
CC	0.2652	0.1042	0.0041	0.6154	0.3512	0.2343	0.2288	0.3478	0.6101
ERGAS	13.1613	13.6754	15.1099	18.2942	10.4265	12.0861	11.4891	10.4729	8.9041
Q-Factor	0.2647	0.1035	0.0024	0.3866	0.3172	0.2175	0.2049	0.3155	0.5476
RASE	52.5005	54.7252	60.4087	73.1577	41.7452	48.3728	45.9754	41.9304	35.6871
RMSE	55.9107	67.89	66.187	90.8438	51.0588	58.7847	55.6489	51.2814	43.1941
Entropy	7.6796	7.6412	7.6477	6.6351	6.8512	7.3431	6.9885	6.8544	7.3095

Erreur Relative Globale Adimensionnelle de Synthese(ERGAS): measures the global dimensional synthesis error, it represents fused image quality.

$$ERGAS = \frac{100}{R}\sqrt{\frac{1}{N}\sum_{K=1}^{N}\left(\frac{RMSE(I_K, J_K)}{\mu(I_K)}\right)^2} \tag{11}$$

R: Resolution index (MS spatial resolution/fused spatial resolution)
$\mu(I_K)$: Mean Radiance of band
Cross Correlation (CC): measure the correlation between fused image and reference image.

$$CC = \frac{\sum_{i=1}^{M}\sum_{j=1}^{N}[F(i,j)-\overline{F}][X(i,j)-\overline{X}]}{\sqrt{\sum_{i=1}^{M}\sum_{J=1}^{N}[F(I,J)-\overline{F}]^2\sum_{i=1}^{M}\sum_{j=1}^{N}[X(i,j)-\overline{X}]^2}} \tag{12}$$

X and F denote the sources of Multispectral image and the fused images
RMSE: Root Mean Square Error measured difference of fused and reference image.

$$RMSE = \left(\frac{\sum_{i=1}^{M}\sum_{j=1}^{N}[I_R(i,j)-I_F(i,j)]^2}{MXN}\right)^{\frac{1}{2}} \tag{13}$$

$I_R(i,j)$: Pixel values of Reference image
$I_F(i,j)$: Pixel value of fused image
Relative Average Spectral Error (RASE): To estimate the global spectral quality of the fused images,

$$RASE = \frac{100}{M}\sqrt{\frac{1}{N}\sum_{i=1}^{N}RMSE^2(B_i)} \tag{14}$$

Here
M = Mean radiance of the N multispectral bands (B_i) of the original image.
N = Number of Bands.

In the MS image in Fig. 3A, cloud information is available in certain bands (band 1, band 3, band 5, band 7, and band 9), and the remaining bands provide no cloud information. The complete cloud information appears in a single band after DR. In Fig. 3B, the maximum cloud information appears in band 1. Supervised and unsupervised classification of NOAA MS images is useful for separating objects based on colour pixels. However, these classification methods fail in case of intensity variation in the same object. In the cloud area, the object appears homogeneous. However, there exist different temperatures when the density is variable. Using the proposed technique, different temperature areas of the same object can be distinguished. The differentiation depends on the thickness of the cloud object.

The classification can be performed using a clustering algorithm. Fig. 4 depicts the classification results with unsupervised classification and the proposed technique. Fig. 4B illustrates the unsupervised classification image. The temperatures of various classes are presented in Table 1b.

Fig. 4B cannot be used to categorize the types of clouds. For separating the cloud-free and cloud contaminated pixels, the previously mentioned techniques are suitable. All the bands contain redundant information. However, some non-Gaussian information also appears when using the proposed technique. Class 5 in the input image represents the cloud information. The surface temperature is not constant throughout the object and can be measured using thermal temperature channels. The cloud-contaminated area can be separated using panchromatic and false color composite image. The different types of clouds cannot be directly distinguished in the input image. Image processing is required to determine the types of clouds. Three classes are obtained using the clustering technique (class 3, class 4, and class 5) on the cloud object and corresponding temperature. The surface reflectance is provided in Table 5. The variation in the surface temperatures of the clouds at different positions of the object can be observed using the clustering technique for the proposed output image (Fig. 5).

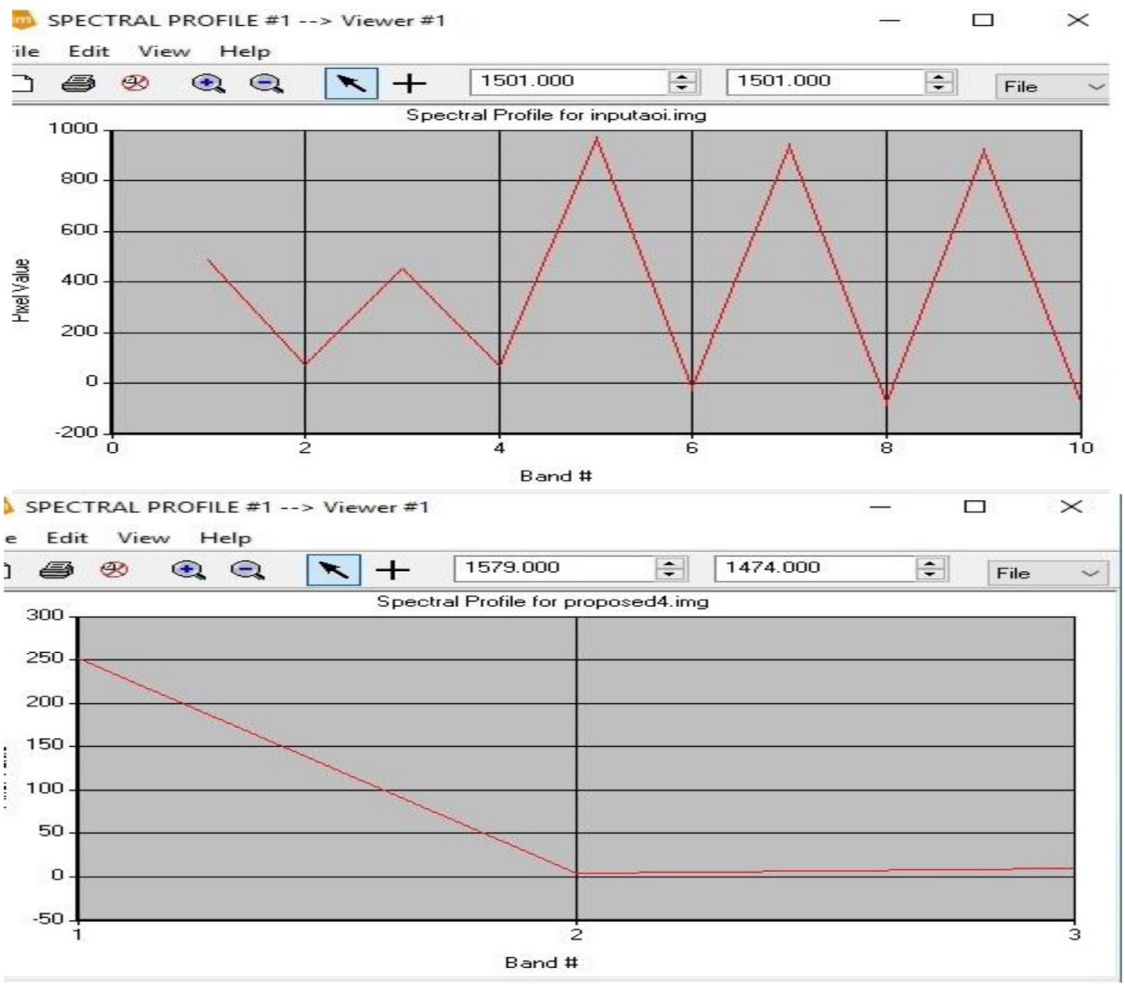

Fig. 3. (A) Cloud spectral information in the input image. (B) Cloud spectral information in the proposed image.

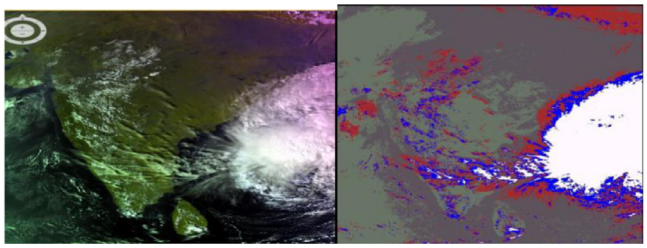

Fig. 4. (A) NOAA MS image. (B) Unsupervised classified image.

Fig. 6A illustrates the proposed output image, and Fig. 6B displays the corresponding supervised classified image. The temperature values of the three new classes change depending on the thickness of the object. These two outputs indicate that supervised classification of the proposed image results in superior object classification (Fig. 7; Table 2).

Tables 3 and 4 indicate the accuracy of the input MS and proposed output images. Unsupervised classification can be performed using the random sample point method, For each sample point, the appropriate type of object is identified from the unsupervised and supervised classification images. Due to its low resolution, the accuracy levels of unsupervised classification are lower than those of the proposed method for the input image. The non-Gaussian classes are easily identified using higher-order statistics ICA operations. The low- and high-frequency components in the image are enhanced through PCA (Table 6).

unsuper.img : Layer_1

Row	Histogram	Color	Red	Green	Blue	Opacity	
0	0		0	0	0	0	Unclassified
1	1959801		0.361	0.325	0.361	1	Class 1
2	1318643		0.408	0.455	0.396	1	Class 2
3	563431		0.647	0.165	0.165	1	Class 3
4	334334		0	0	1	1	Class 4
5	563071		1	0.973	1	1	Class 5

Fig. 5. Screenshot of the unsupervised object classes from ERDAS imagine.

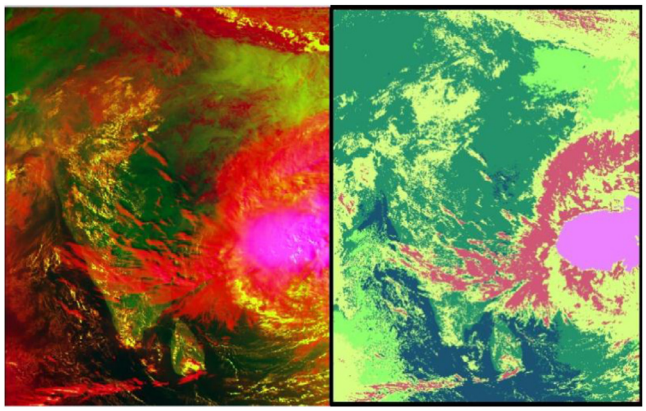

Fig. 6. (A) Proposed image (B) Supervised classified output image.

supervised2.img : Layer_1

Row	Histogram	Color	Red	Green	Blue	Opacity	
0	0		0	0	0	0	Unclassified
1	176368		0.925	0.51	1	1	cloud1
2	1456680		0.839	1	0.506	1	cloud2
3	504722		0.824	0.341	0.467	1	cloud3
4	400082		0.565	1	0.424	1	cloud4
5	478081		0.106	0.325	0.451	1	cloud free1
6	1723347		0.141	0.576	0.424	1	cloudfree 2

Fig. 7. Attribute table for the supervised classification of the proposed image.

Table 2
Surface temperature for the unsupervised classes.

S. No	Class	Surface temperature (°C)
1	Class 1	20
2	Class 2	25
3	Class 3	−1 to 7
4	Class 4	−24
5	Class 5	−80 to −85

Table 3
Accuracy assessment table for the unsupervised classification of the input image.

Class name	Reference Total	Classified Total	Number Correct	Producer Accuracy	User Accuracy	Kappa
Class 1	100	108	96	**96.00%**	**88.89%**	**0.8177**
Class 2	72	71	58	**80.56%**	**81.69%**	**0.7453**
Class 3	37	33	26	**70.27%**	**78.79%**	**0.752**
Class 4	16	11	7	**43.75%**	**63.64%**	**0.6121**
Class 5	31	33	29	**93.55%**	**87.88%**	**0.8621**

Overall classification accuracy = 84.38%.
Overall kappa statistics = 0.7831.

Table 4
Accuracy assessment of supervised classification of the proposed image.

Class name	Reference Totals	Classified Totals	Number Correct	Producer accuracy	User accuracy	Kappa
Thick cloud	10	11	10	**100.00%**	**90.91%**	**0.9053**
Low/middle Thick cloud	75	78	66	**88.00%**	**84.62%**	**0.7802**
Thin cloud	9	14	8	**88.89%**	**57.14%**	**0.5554**
Thin cloud over ground	25	26	21	**84.00%**	**80.77%**	**0.7863**
Water	25	24	23	**92.00%**	**95.83%**	**0.9537**
Land	96	97	86	**89.58%**	**88.66%**	**0.8159**

Overall classification accuracy = 85.6%.
Overall kappa statistics = 0.8037.

This classification results taken from ERDAS imagine tool, with reference of confusion matrix the classification accuracy and kappa statistics values are noted. The classification can be done by using confusion matrix, using this identified the number of correctly and incorrectly mapped in classified sites, The diagonal values represent the correctly matched sites, other sits are occupied in another class.

$$\text{Theoverallaccuracy} = \text{Numberofcorrectlyclassifiedsites/totalnumberofreferencesites} \tag{15}$$

$$\text{Kappastatistics} = K = (p_o - p_e)/(1 + p_e) \tag{16}$$

P_e= the probability of random agreement
P_o= The observed proportionate agreement

Image classification is an efficient method of extracting information from an image. Accuracy assessment is used to determine the reliability of a classified image. Classification can be performed with an error matrix (confusion matrix). The matrix is filled with values obtained from a random sample. The accuracy levels are determined using reference data. The evaluation of the classification depends on the overall accuracy, user accuracy, producer accuracy (PA), and kappa coefficient. The values of the aforementioned parameters depend on the number of matched and missed samples. Using total accuracy finding average summary even error was distributed between objects. Avoid this problem using the PA, user accuracy, and kappa coefficient. The user accuracy corresponds to the error of commission, and the PA corresponds to the errors of omission. The kappa coefficient indicates the difference between the actual agreement and the agreement expected by chance. The PA indicates the number of correctly classified pixels in a particular class, that is, the percentage of pixels actually belonging to that specific class in the image. The user accuracy, which is referred to as the reliability, indicates the possibility of a class on the map actually being present on the ground.

4.1. Cloud identification of NOAA MS images by using channel reflections and temperature values

AVHRR MS images from the day-time orbits of NOAA-14 were downloaded from the high resolution picture transmission receiver located at Sri Venkateswara University, Tirupati. Five channels with a 1.1 km resolution were obtained. The visible channel (Ch1) was used to measure the reflectance because it detected solar reflected radiance. The thermal channels (Ch3, C4, and Ch5) were used to measure the surface temperature and earth-emitted radiance [5].

The total input selected area was considered as cloud contaminated and cloud free. Cloud-free areas are required for vegetation studies. According to the reflectance, the clear-sky pixels were classified as land areas, barren land areas, and water areas. Depending on the shape, reflectance, density, and colour of the clouds, the area could be categorized as thick cloud, thin clouds, cirrus, cloud edge, and cloud shadow. Due to high solar reflectance, the thick clouds appeared as white [28]. Depending on their densities, the thin clouds appeared as various shades of gray. This study focused on the types of cloud in the cloud-contaminated areas. Due to the difficulty in identifying them, cloud shadows were treated as cloud-contaminated pixels. Which minimizes/maximize cloud contamination. These images are not completely cloud free. Due to misidentification, land pixels, unidentified cloud shadow pixels, and water pixels do not exhibit accurate results. A cloud

Table 5
NOAA-AVHRR MS image albedo and thermal channel values.

Cumulonimbus cloud	Ch 1 Reflectance (%)	Ch 2 Reflectance (%)	Ch 3 Temperature (°C)	Ch 4 Temperature (°C)	Ch 5 Temperature (°C)
	77.455	71.71	−15.5	81.17	82.40
	73.116	67.49	−20.813	87.499	88.696
	79.151	74.076	−15.152	78.130	79.173
	72.830	67.36	−16.87	79.604	80.737
Cirrus based cloud	Ch 1 Reflectance (%)	Ch 2 Reflectance (%)	Ch 3 Temperature (°C)	Ch 4 Temperature (°C)	Ch 5 Temperature (°C)
(high level cloud)	63.49	53.00	25.36	13.322	10.19
	69.2	49.7	20.4	13.32	9.502
	70.14	52.827	18.733	7.122	4.730
	75.4	59.9	6.399	−14.386	−17.022
	63.2	53.4	14.29	0.078	0.114
	85.92	67.6	0.925	−17.17	−19.7
Middle level clouds	Ch 1 Reflectance (%)	Ch 2 Reflectance (%)	Ch 3 Temperature (°C)	Ch 4 Temperature(°C)	Ch 5 Temperature(°C)
	36.63	33.49	−0.22	−27.5	−30.0
	31.6	25.9	4.54	−20.4	−24.0
	43.304	37.4	−3.5	−34	−37.971
	50.8	43.98	−10.038	−37.0	−38.554
	22.5	14.7	31.2	21.71	18.40
	26.171	21.2	14.628	−4.5	−8.706
	Ch 1 Reflectance (%)	Ch 2 Reflectance (%)	Ch 3 Temperature (°C)	Ch 4 Temperature(°C)	Ch 5 Temperature(°C)
Thin cloud on ground	23.112	16.759	21.885	19.523	17.420
	26.72	19.79	21.71	18.57	16.11
	23.90	16.36	22.54	19.714	17.6
	24.71	17.93	20.43	18.116	15.56
	21.96	16.029	23.35	20.327	18.151
Ground	Ch 1 Reflectance (%)	Ch 2 Reflectance (%)	Ch 3 Temperature (°C)	Ch 4 Temperature(°C)	Ch 5 Temperature(°C)
	12.2	18.7	27.8	26.7	24.8
	10.6	17.14	28.6	25.5	22.4
	6.4	16.1	25.9	23.9	21.18
	18.2	20.0	29.51	25.2	25.01
Water	Ch 1 Reflectance (%)	Ch 2 Reflectance (%)	Ch 3 Temperature (°C)	Ch 4 Temperature(°C)	Ch 5 Temperature(°C)
	5.6	2.30	24.8	22.8	19.0
	5.104	2.010	25.7	23.3	19.7
	4.467	1.931	25.276	23.70	20.7
	14.52	7.2	20.5	19.4	18.8
	8.7	3.8	25.3	22.4	19.3

Table 6
NDVI and reflectance ratio for the classified objects.

Object	NDVI	Reflectance ratio Q = R2/R1
Cloud	−0.044	0.92
Low level cloud on land	−0.191	0.72
Land	0.431	1.16
Water	−0.3	0.4

free image is obtained by using the threshold method on time series images or the MVC technique [6]. The cloud-free image can be applied for various research purposes, such as environmental applications. The identification of water pixels can be improved using Ch-4 brightness temperature (BT) [7].

The normalized difference vegetation index (NDVI) of AVHRR images is used for vegetation index determination, biomass estimation, and land cover mapping. The NDVI and surface reflectance(albido) are used to separate the cloud-contaminated and cloud-free areas [4]. The maximum NDVI value is assigned to minimize the effect of cloud free data, whereas low NDVI values are assigned to the cloud contaminated areas (snow, smoke, clouds, and ice) [14]. The results of the proposed algorithm object were verified using the BT, solar reflectance, and solar reflectance ratio of different channels, the BT difference between channels; and NDVI values. By using these parameters, cloud-contaminated pixels could be separated from the clear-sky pixels for vegetation studies. The sensors observed both the ground and clouds when a thin partial cloud appeared above the ground. The reflectance and temperatures depended on the fraction of cloud. Many algorithms have been developed for the identification of clouds by using surface in homogeneity, threshold and split windowing. The total cloud cover can be classified into the thick cloud, thin cloud, cirrus, and cloud edges categories according to the colour, shape, density, and reflectance The NDVI and BT values were recorded for each sample on the cloud.

Separating the cirrus form clouds and water level formed clouds by using the thermal channels is difficult. The total cloud-contaminated area can be divided into four categories, namely high level clouds (cumulonimbus), cirrus form clouds, middle-level clouds, and low-level clouds. The middle-level clouds form with high ice crystals and water levels. The ice reflectance in middle-level clouds is higher than that in water-level clouds. Middle-level clouds are formed by water vapor and have very low visible and IR reflectance values compared with those of the cirrus-form clouds. The thin layer cloud over the ground has very low reflections in Ch 1 and Ch 2 and positive temperature values at ground levels. By using the proposed algorithm, the different cloud types as well as the non-Gaussian objects can be identified.

The NDVI and reflection ratio of Ch 2 and Ch 1 enable the cloud-free and cloudy pixels to be identified. Cloud-free pixels have a Q-value higher than 1, and cloudy pixels have a Q-value between 0.75 and 1. Due to the low reflection in the NIR channel, the Q-value of the cloud is very low. The NDVI values are nearly 0 for cloudy areas, very low for water, and very high for land areas.

5. Conclusion

The MS image enhancement technique is very useful in remote sensing applications [23]. Instead of studying all the channels, the image processing technique is applied after removing redundant information by using ICA and PCA. The proposed technique can be used for satellite data compression and enhancing the spatial and spectral features of MS images to better classify objects. The spatial and spectral parameters of the output image obtained with the proposed method are superior to those obtained with PCA, HIS, DWT-ICA techniques. The output image also exhibits good classification accuracy. The proposed algorithm is suitable for DR, colour image enhancement, and classification for separating thick, middle, thin clouds and cloud free objects with good accuracy.

Acknowledgment

The authors are grateful to the Department of Electronics and Communication engineering and Technical Education Quality Improvement Programme, Phase III & Center of Excellence [TEQIP 1.2.1 (CoE)], Sri Venkateswara University College of Engineering, for providing NOAA satellite images of L-band receiver, and simulators for this Research.

References

[1] Haralick RM, Shanmugam K, Dinstein I. Textural features for image classification. IEEE Trans Syst Man Cybern 1973;SMC-3:610–21.
[2] Byrne GF, Crapper PF, Mayo KK. Monitoring land cover change by principal component analysis of multitemporal Landsat data. Remote Sensing Environ 1980;10:175–84.
[3] Kuo KS, Welch RM, Sengupta SK. Structural and textural characteristics of cirrus clouds observed using high spatial resolution Landsat imagery. J Appl Meteorol 1988;27:1242–60.
[4] Allen RC, Durkeea PA, Wash CH. Snow/cloud discrimination with multispectral satellite measurements. J Appl Meteorol 1990;29:994–1004.
[5] Baum BA, Wielicki BA, Minnis P. Cloud-property retrieval using merged HIRS and AVHRR data. J Appl Meteor 1992;31:351–69.
[6] Peak JE, Tag PM. Segmentation of satellite imagery using hierarchical thresholding and neural networks. J Appl Meteor 1994;33:605–16.
[7] Gao B-C, Wiscombe WJ. Surface-induced brightness temperature variations and their effects on detecting thin cirrus clouds using IR emission channels in the 8-12 μm region. J Appl Met 1994;33:568–70.

[8] Hutchison KD, Locke JK. Snow cover identification through cirrus-cloudy atmospheres using daytime AVHRR imagery". Geophys Res Lett 1997;24(14):1791–4.
[9] Kim YT. Contrast enhancement using brightness preserving bi-histogram equalization. IEEE Trans Consum Electron 1997;43:1–8.
[10] Muresan DD, Parks TW. Adaptive principal components and image denoising. In: Proceedings of the 2003 international conference on image processing, 1; 2003. p. 1101–4.
[11] Pandit VR, Bhiwani RJ. Image fusion in remote sensing applications: a review. Int J Comput Appl 2015;120(10):22–32.
[12] Wang J, Chang C-I. Independent component analysis-based dimensionality reduction with applications in hyperspectral image analysis. IEEE Trans Geosci Remote Sensing 2006;44(6):1586–600.
[13] Patra SK, Shekher M, Solanki SS, Ramachandran R, Krishnan R. A technique for generating natural colour images from false colour composite images. Int J Remote Sensing 2006;27:2977–89.
[14] Tang Q, Oki T. Daily NDVI relationship to cloud cover. Am Meteorol Soc 2007;46:377–87.
[15] Wang Z, Boesch R. Color- and texture-based image segmentation for improved forest delineation. IEEE Trans Geosci Remote Sensing 2007;45:3055–62.
[16] Ilsever M, Unsalan C. Pixel-based change detection methods, remote sensing applications. Springer Briefs in Computer Science; 2012. p. 7–21.
[17] Kaur R, Ganju A. Cloud classification in NOAA AVHRR imageries using spectral and textural features. J Indian Soc Remote Sens 2008;36:167–74.
[18] Ye Z, Mohamadian H, Pang SS, Iyengar S. Contrast enhancement and clustering segmentation of gray level images with quantitative information evaluation. WSEAS Trans. Inform Sci Appl 2008;5(2):181–8.
[19] Ehlers M, et al. In: Bebis G, et al., editors. Multi-image fusion in remote sensing: spatial enhancement vs. spectral characteristics preservation. ISVC Part II; 2008. p. 75–84.
[20] Laban N, Nasr A. Spatial cloud detection and retrieval system for satellite images. Int J Adv Comput Sci Appl 2012;3(12):212–17.
[21] Ahmad A. Comparative analysis of supervised and unsupervised classification on multispectral data. Appl Math Sci 2013;7:3681–94.
[22] Ghabousian R, Allahbakhshi N. Survey of contrast enhancement techniques based on histogram equalization. Int J Rev Life Sci 2015;5(8):901–8.
[23] Janani P, Premaladha J;, Ravichandran KS. Image enhancement techniques: a study. Indian J Sci Technol 2015;8(22):1–12.
[24] Shereena VB, Julie MDavid. Significance of dimensionality reduction in image processing. Signal Image Process Int J (SIPIJ) 2015;6(3):27–42.
[25] Singh RP, Dixit M. Histogram equalization: a strong technique for image enhancement. Int J Signal Process Image Process Pattern Recognit 2015;8:345–52.
[26] Venkata Krishnamoorthy T, Umamaheswara Reddy G. Noise detection using higher order statistical method for satellite images. Int J Electron Eng Res 2017;9(1):29–36.
[27] Venkata Krishnamoorthy T, Umamaheswara Reddy G. Fusion enhancement of multispectral satellite image by using higher order statistics. Asian J Sci Res 2018;11:162–8.
[28] Venkata Krishnamoorthy T, UmamaheswaraReddy ProfG. Cloud identification method using HOS based ICA for multispectral NOAA image. I-manager's J Future Eng Technol 2018;13:35–41.
[29] George J. Fundamentals of remote sensing. 2nd ed. Universities Press; 2011.
[30] . In: Kidwell KB, editor. NOAA polar orbiter data user's guide. NOAA National Environmental Satellite Data and Information Service; 1991. p. 120. Available from 151 Patton Ave., Asheville, NC 28801-5001.
[31] Petrou M, Bosddogianni P. Image processing: the fundamentals. UK: John Wiley and Sons, Inc.; 2000. p. 335. ISBN 0-471-99883-4.
[32] Gonzalez RC, Woods RE. Digital image processing. 3rd ed. Prentice-HallEnglewoodCliffs; 2002.

T. Venkata Krishnamoorthy is a Research Scholar in the Department of Electronics and Communication Engineering at Sri Venkateswara University, Tirupati, Andhra Pradesh, India. He has completed B.Tech in Electronics and Communication Engineering from JNT University, Hyderabad, India and M.Tech in Communication and Signal Processing from Sri Krishnadevaraya University, Anantapur, India. He has Teaching & Industrial Experience of 6 years. His areas of Interest are Image and Signal Processing. He is a lifetime memberof ISTE.

G. Umamaheswara Reddy is currently working as a Professor in the Department of Electronics and Communication Engineering at Sri Venkateswara University, Tirupati, Andhra Pradesh, India. He has completed B.Tech in Electronics and Communication Engineering, M.Tech in Instrumentation and Control Systems, and obtained Ph.D. from Sri Venkateswara University,Tirupati, India. He is a member of ISTE, IE, and BMSI. He has a teaching experience of more than 20 years and has 16 technical publications in National & International Journals.His areas of interest include Signal Processing and Biomedical Signal Processing.